Improving the compressive response of bio-polymeric additively manufactured cellular structures via foam-filling: An experimental and numerical investigation

A. Corvi, L. Collini & C. Sciancalepore

Published online: 12 Aug 2023.

Submit your article to this journal ↗

View related articles ↗

View Crossmark data ↗

Taylor & Francis
Taylor & Francis Group

Check for updates

ORIGINAL ARTICLE

Improving the compressive response of bio-polymeric additively manufactured cellular structures via foam-filling: An experimental and numerical investigation

A. Corvi [ID], L. Collini [ID], and C. Sciancalepore [ID]

Department of Engineering and Architecture, University of Parma, Parma, Italy

ABSTRACT

Additive Manufacturing is effective at addressing advanced innovative design requirements for functional applications. Lattice structures and lightweight composites are the result of engineering designs for enhanced mechanical and structural properties. Inspired by nature, this work investigates the static and cyclic compressive response of 3D-printed Triply-Periodic-Minimal-Surface cellular structures made of Poly-(Butylene-Adipate-*co*-Terephthalate) (PBAT) biopolymer functionalized with Poly-Urethane foam. The plateau stress of the hybrid structure is 30% higher and the specific energy absorption capability 18% higher than the empty structure due to interaction between the two phases. A finite-element model is developed as a supporting tool to analyze, predict, and optimize structural behavior, as well as improve understanding of the deformation mechanisms. In addition, PBAT proves to be the ideal candidate for greener manufacturing, combining good mechanical properties with biodegradability, paving the way for a range of new applications.

GRAPHICAL ABSTRACT
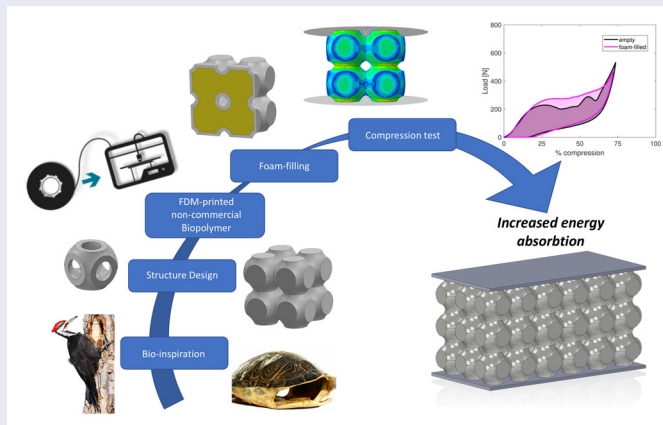
1. Introduction

Additive Manufacturing (AM) has recently taken on an important role in the production of advanced structures thanks to its capability of embracing complex designs that would otherwise be impossible to obtain with traditional subtractive or forming technologies. Lattices and Triply Periodic Minimal Surface (TPMS) structures, often referred to in the literature as Mechanical Metamaterials (MM), are the result of this capability of re-designing structural and functional components to obtain superior properties [1–3]. Over recent years, lightweight structures with enhanced mechanical behavior have paved the way for new multifunctional applications in many engineering disciplines, including biomechanical [4–5], aerospace, acoustic [6] and energy storage [7–9]. Numerical tools aiding design and structural optimization have also become of primary importance

thanks to their role in both adopting highly innovative designs [10] and predicting structural behavior [11].

Amongst the various AM technologies, the most widely employed is known commercially as Fused Deposition Modeling (FDM). This process consists of extruding and subsequently depositing a polymeric filament in a semi-molten state. Lattices and TPMS structures produced *via* FDM with thermoplastic polymers have recently attracted increasing attention. Within this framework, most applications exploit their compressive behavior [3, 12–15], ranging from lifestyle products [16] to crashworthy structures [17–19].

Focusing on the unique energy absorption features of such structures, a secondary material, typically foam-like, is often employed to enhance the mechanical response under compressive loads [20–24]. Roudbeneh [25] demonstrated an increase in energy absorption of up to 50% with PU-

filled honeycomb sandwich panels, yielding substantial benefits in terms of damage appearance. Gel filler materials [26–27] and water [28] have also been investigated recently, providing enhanced energy absorption capabilities and demonstrating a damping effect during impact loading, respectively. Furthermore, shear-thickening fluids [29] allow the dynamic response to be tailored depending on the fluid shear rate, with interaction between the geometry and fluid varying as function of the impact velocity. Poly-Urethane (PU) foams make up the largest portion of polymeric foams. Their combination of low weight and good thermo-mechanical properties make them ideal candidates as thermal and sound insulators, as well as useful materials for advanced mechanical applications [30–31].

Filling thin-walled structures with PU foam is often associated with a significant increase in the energy absorption capability of the assembly. Yao [32] and Ren [33] reported beneficial interactions between the foam and external shells of aluminum and stainless-steel auxetic tubes, respectively, demonstrating significant improvements in response compared to the sum of the individual contributions of each constituent. Recently, foam-filled 3D-printed lattice structures have also combined the effects of novel designs and optimized structures with that of the filler [34–36]. Miralbes [37] compared the experimental responses of different TPMSs in a hybrid foam-filled configuration, demonstrating that foam delays onset of the densification regime at high strain and reduces layer-by-layer failure of the structure. The properties of foam-filled cellular structures created via multi-material AM has also been investigated experimentally [38], with structures exhibiting enhanced stiffness and energy dissipation compared to empty and equivalent-weight structures. However, these encouraging findings are related to experimental evidence and lack full investigation into the deformation mechanisms at play.

Within this context, the present work provides greater insight into the deformation mechanism of such structures and discusses possible tools to analyze and improve their functional performance. A PBAT 3D-printed walled cellular structure is investigated under static and cyclic compressive loading in two configurations, empty and filled with PU foam. Attention is placed on the stress field that develops during compression and the consequent global deformation of the structure, responsible for its overall mechanical performance. The enhanced energy absorption capability of PU-filled structures is discussed in terms of the interaction between the two constituent phases, with this phenomenon influencing the resulting performance in a beneficial way. A Finite-Element (FE) model is developed to better understand the stress distribution within the structure. Simulation outputs are compared with experimental data in terms of the resulting mechanical response and structural deformation, with good alignment achieved between the two.

Further to these outcomes, a novel material is introduced, comprising a noncommercial Poly-(Butylene Adipate-co-Terephthalate) (PBAT) biopolymer filament that is extruded and printed via FDM. Thanks to its promising properties, PBAT is a good candidate for the production of components that combine good mechanical performance in new applications [39] with more environmentally friendly manufacturing [40]. PBAT is a thermoplastic polyester that is gaining significant importance due to its biodegradability in conjunction with good mechanical properties. High flexibility and relatively low elastic modulus make PBAT easily processable as a filament for the production of very flexible parts via 3D printing, replacing non-biodegradable oil-based flexible filaments that are currently commercially available.

2. Materials and Methods

2.1. Structure geometry

Inspiration for this work was found in the natural world, where structures with multifunctional properties are the result of adaptation of species over millions of years. Focusing on energy absorption properties, such as those observed in turtle shells and woodpecker skulls, the use of a secondary material, typically foam-like, is often involved to enhance the mechanical response of a structure, see Figure 1a. Within the present work, a Schwarz primitive lattice (P-lattice) with 10x10x10 mm unit cell and 0.8 mm shell thickness was employed. A periodic structure was created via face-to-face tessellation of this unit cell, as shown in Figure 1b. External walls with 0.8 mm thickness were added to the resulting structure to generate a closed volume suitable for filling with a secondary material.

Specimens comprising 2x2x2 cell arrays were printed with the aim of achieving a reasonable printing time in the order of 2.5–3 h. The effectiveness of specimens in representing periodic structures is discussed in Section Scalability of results, where two specimens comprising 3x3x3 cell arrays were also printed and tested to assess scaling effects.

To perform the filling process, a modified G-code file was used for 3D printing that included a pause in extrusion just before the top printed layer at 19.2 mm height. At this point, foam was sprayed inside the cell cavity to fill the whole volume, after which printing was resumed. The process was performed quickly so as to avoid significant cooling of the filament, ensuring high-quality adhesion between the top layer and the previously deposited one.

The value of relative density, ϕ, the most significant parameter for designing cellular and lattice structures, was set via Equation (1) within the range proposed by Ashby [41] for "cellular solids" in nature, defined as $\phi < 0.3$.

$$\phi = \frac{\rho^*}{\rho_s} = \frac{\rho_{lattice}}{\rho_{solid}} = 0.26 \qquad (1)$$

2.2. Material characterization

PBAT is a semicrystalline thermoplastic polymer characterized by significant ductile and stretchy behavior. Its biodegradability has led it to emerge as a leading flexible bioplastic [42]. PBAT combines some of the beneficial attributes of synthetic and bio-based polymers. Comprising two repeating units, butylene terephthalate (BT) and
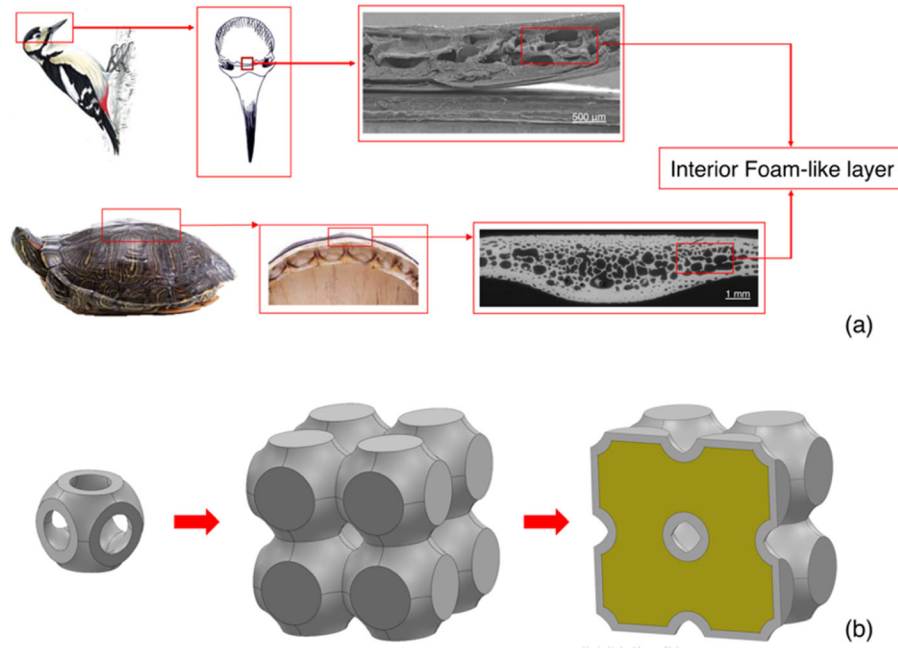
Figure 1. a) Inspiration from nature for multiphase composites exhibiting enhanced energy absorption; b) Structure definition via tessellation of unit cell and addition of walls.

butylene adipate (BA), linked together by a condensation reaction, PBAT is derived from common petrochemicals yet is biodegradable. Its properties depend on the molar ratio of the two constituents. As a synthetic polymer, it can readily be produced at large scale, possessing physical properties needed to make flexible films that rival those made of conventional plastics [43].

Thanks to its useful properties, PBAT has recently been introduced into the world of 3D printing. In the present work, PBAT pellets supplied by MAgMa Spa (Italy) in the form of white granules (PBAT Ecoworld), were used to create a filament suitable for printing *via* a single screw extruder (Felfil Evo, Felfil, Italy). The system included multiple fans to cool the polymer and a spooler and optical sensor, shown in Figure 2, to regulate the filament diameter and obtain a constant value. The extrusion temperature was set to $150 \pm 10\,^\circ\text{C}$ and the screw angular velocity maintained at 3 rpm. The target value for the filament diameter was fixed at $1.65 \pm 0.10\,\text{mm}$.

A BQ Hephestos-2 3D printer with $0.6\,\text{mm}$ extruder nozzle was employed for experiments. The printer head temperature was set to $180\,^\circ\text{C}$, the printing velocity to $20\,\text{mm/s}$, and the layer height to $0.2\,\text{mm}$.

Mechanical characterization of the 3D printed material was performed by subjecting FDM-printed specimens with standard UNI EN ISO 527 and 1BA geometry to uniaxial tensile tests on a TesT dynamometer (Model 112, 2 kN cell load, TesT GMBH Universal Testing Machine, Germany) at a crosshead velocity of 50 mm/min. The material behavior is reported in Figure 3a, exhibiting an initial linear elastic response up to the onset of yielding followed by a wide plastic "plateau" region at large strain.

Commercial PU foam was employed to fill the cellular structures produced by FDM. The density of this material was determined experimentally as $\rho_{foam} = 47.2\,kg/m^3$. Cylindrical samples were subject to compression tests for

mechanical characterization with a height-to-radius ratio $H/R = 1$ and dimensions suitable to consider porosity within samples as being homogeneous. The outcomes of compression tests are reported in Figure 3b.

2.3. Numerical modeling

A Finite-Element (FE) model was developed with the commercial software Abaqus© to simulate the mechanical response of foam-filled cellular structures. Numerical model outputs in terms of macroscopic deformation and load-displacement curves were compared with experimental outcomes. PBAT was modeled with an elasto-plastic constitutive model in line with the characteristics discussed in Section Material characterization, setting Young's modulus as $E = 60\,MPa$ and Poisson' ratio as $\nu = 0.46$ (computed *via* Digital Image Correlation (DIC) analysis), and defining the plastic regime based on the test data presented in Figure 3a. As the behavior of PU foam was observed to be hyper-elastic, this material was modeled with the HyperFoam constitutive model, in which the strain energy density function, U, is expressed in terms of the principal stretches, as reported in Equation (2). Numerical fitting of test data and the numerical model was performed in the Abaqus© environment, with a HyperFoam model of 3rd degree found to be the most accurate, see Figure 3b. Table 1 lists the coefficients employed for the simulations, with β representing the compressibility of the foam, defined as $\beta = \nu/(1 - 2\nu)$.

$$U = \sum_{i=1}^{N} \frac{2\mu_i}{\alpha_i{}^2} \left[\hat{\lambda}_1{}^{\alpha_i} + \hat{\lambda}_2{}^{\alpha_i} + \hat{\lambda}_3{}^{\alpha_i} - 3 + \frac{1}{\beta} \left(J_{el}{}^{-\alpha_i \beta} - 1 \right) \right] \quad (2)$$

Numerical analysis was performed in the Abaqus Explicit environment. *General Contact* was employed for contact between the top and bottom faces of the cellular structure
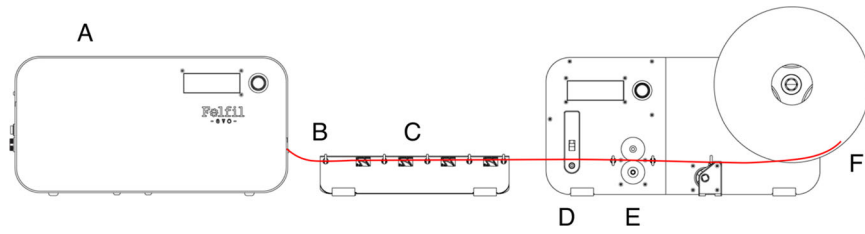
Figure 2. PBAT extrusion line schematic: A – extruder; B – wire extrusion head; C – air cooling system; D - optical sensor; E - filament pull spools; F - filament winder.
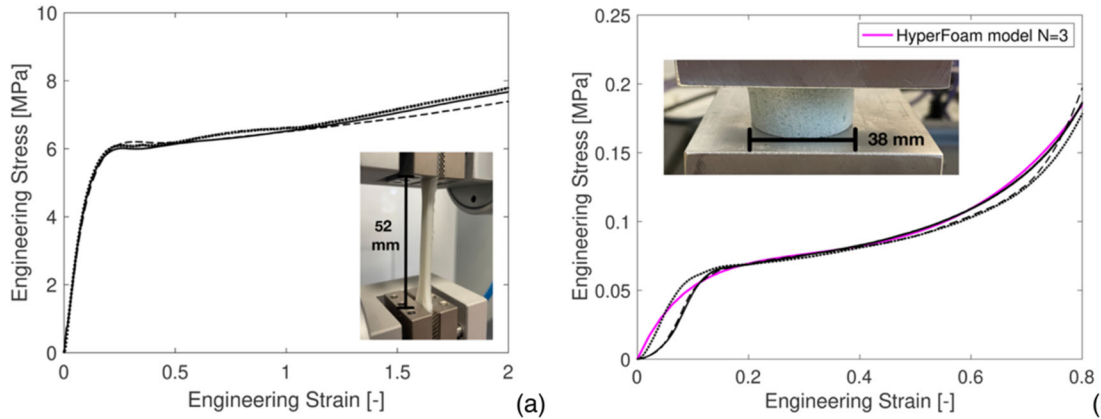

Figure 3. a) Tensile test response of 3D-printed PBAT; b) Compressive behavior of PU foam.

and the respective compressive plates, as well as for contact between different parts of the structure during the compression process. "Hard contact" was defined in the normal direction, while tangential behavior was modeled with a "penalty" function and a friction coefficient of 0.2. Both the upper and lower plates were modeled *via* analytically rigid surfaces. Linear C3D4 elements were adopted, as shown in Figure 4a, with the mesh size chosen to achieve independence of results during convergence analysis. Mass scaling with a factor of 10 was employed over the whole model to scale the minimum solution increment, with no loss of physical meaning. A *TIE constraint was set between the cell internal surface and the external surface of the foam, as shown in Figure 4b. Any detachment of the shell and foam was thus avoided, in line with experimental outcomes where specimens that were sectioned after deformation were found

to have maintained perfect adhesion between the foam and shell.

2.4. Performance parameters

Both empty and Foam-Filled (FF) configurations were tested experimentally and numerically under compression loading at a displacement rate of 5 mm/min [33]. The resulting curves were compared to determine the contribution of the foam to the load-carrying capacity. Cyclic loading was also applied to investigate the transient behavior of the material. The total energy absorption (TEA) and total energy dissipation (TED) capabilities were defined as per Equation (3), where F represents the applied load and x_0 and x_f the displacement at the first and final stages, respectively:

$$TEA = \int_{x_0}^{x_f} F(x)dx \quad TED = \oint_{x_0}^{x_f} F(x)dx \tag{3}$$

To compare the two configurations, it was necessary to introduce the absorbed and dissipated energy per unit mass, or specific energy absorbtion (SEA) and dissipation (SED),

Table 1. Coefficients employed in HyperFoam model.

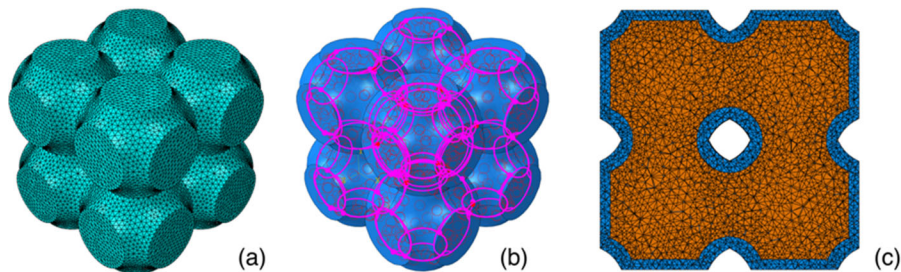|	μ_i	α_i	β
$i = 1$	−0.200436	9.09239	
$i = 2$	0.205346	9.09473	1.16666
$i = 3$	0.443730	−9.14177	

Figure 4. Numerical model: a) Mesh of the external shell; b) *Tie constraint between the shell and foam; c) Foam mesh.

respectively, as well as the damping capacity per unit of mass, or specific damping capacity (SDC), as per Equation (4):

$$SEA = \frac{TEA}{M} \quad SED = \frac{TED}{M} \quad SDC = \frac{TED}{TEA} \quad (4)$$

Stress analysis of thin-walled structures can be approached by adopting a stress linearization technique. To compute linearization, the stress field over defined sections must be considered. These sections are referred to as stress classification planes (SCPs). The limit for two opposite sides of an SCP with infinitesimal distance between them is a Stress Classification Line (SCL), which is a straight line that cuts through a section of the component.

The Structural Stress Method was adopted in the present study, as it is the most frequently adopted technique for stress linearization. In this method, stress components are integrated along SCLs through the wall thickness, t, to determine the membrane and bending stress components, defined as:

$$\sigma^m = \frac{1}{t} \int_{-t/2}^{t/2} \sigma \; dx \quad \sigma^b = \frac{6}{t^2} \int_{-t/2}^{t/2} \sigma \; x \; dx \quad (5)$$

2.5. Sample representativity

As the considered solid was a cellular structure based on spatial face-to-face tassellation of a unit cell, it was of primary importance to determine the scalability of the findings. It was therefore necessary to verify that the considered configuration was a significant reference volume describing the response of a much larger component in real applications. During experiments, it was not possible to determine the error introduced by border effects due to the finite geometry. To this end, a validation method was developed, testing structures with varying cell layers and:

i. Comparing the increase in energy dissipation capability due to filling with foam;
ii. Checking if any significant anomalies occurred in the elastic response of the structure.

To obtain the stress-strain curve of the overall compressive response, the nominal compressive stress $\sigma_{N,c}$ and nominal compressive strain $\varepsilon_{N,c}$ are defined as follows:

$$\varepsilon_{N,c} = \frac{-u_c}{h_0} \quad \sigma_{N,c} = \frac{P_c}{A_{0,eq}} \quad (6)$$

where P_c is the compressive load, u_c the nominal displacement, and h_0 the initial height of the structure. $A_{0,eq}$ represents the equivalent cross-sectional area of the structure, described in Equation (7), where V_L is the volume of the lattice structure:

$$A_{0,eq} = \frac{V_L}{h_0} = \phi \cdot h_0^2 \quad (7)$$

The initial stiffness, K_0, of structures with different sizes was also calculated to check if the macro-scale elasticity

exhibited signficiant differences. To obtain the initial stiffness, the crosshead displacement of the test machine in the z-direction and the reaction forces measured by the load cell were considered:

$$K_0 = \left. \frac{dF_T(z)}{dz} \right|_{(\varepsilon=0.05)} \quad (8)$$

where F_T is the total load during the test. Differentiation of $F_T(z)$ was performed from 0.05 strain onwards to neglect the initial part where the elastic behavior was not linear due to inaccuracies in the sample geometry resulting from the printing process.

3. Results and discussion

3.1. Static loading and stress field investigation

The response of empty and foam-filled (FF) lattice structures under static compression is shown in Figure 5a for compression up to 65%. Numerical simulations are also plotted in the same figure. The FF technique led to an increase in the load-carrying capacity at the end of the initial linear response. At small values of compression, the additional strength provided by the foam was negligible due to its hyper-elastic behavior. At increasing compression, the difference between the responses of empty and FF structures became significant, with the latter characterized by a higher load carrying capacity over the plateau region. Within this deformation range, the empty configuration exhibited a fluctuating curve due to instabilities in the cell walls, whereas the foam-filled structure produced almost uniform behavior, stabilizing the load at between approximately 25% and 50% strain.

Alignment between the load-displacement curves obtained with FE simulations and experiments was good, successfully validating the numerical model. Deformation of the structure was also reproduced correctly by the simulation, as shown in Figure 5b, where the stress distribution is shown for both configurations at nominal compression values of 0%, 15%, 27%, 35% and 40%. The structure underwent a very different deformation field in the two tested configurations, with the PU foam acting as a constraint for transverse displacement, preventing inward/outward bending of the cell wall. Consequently, the stress distribution in the external wall was also very different. In particular, filling the inner cavity with foam generated overall regular deformation of the structure, even with significant levels of compression, hence leading to a more isotropic stress distribution in the wall.

The empty configuration was severely affected by the collapse of the upper cell layer, which completely lost its load-bearing capacity while the bottom layer was only slightly deformed. The reduction in anisotropy achieved with foam is clearly visible in Figure 6, where the axial stress of two layers of cells is compared for increasing levels of nominal compression. These outcomes highlight the fact that the benefits of filling lattice structures with foam go beyond the
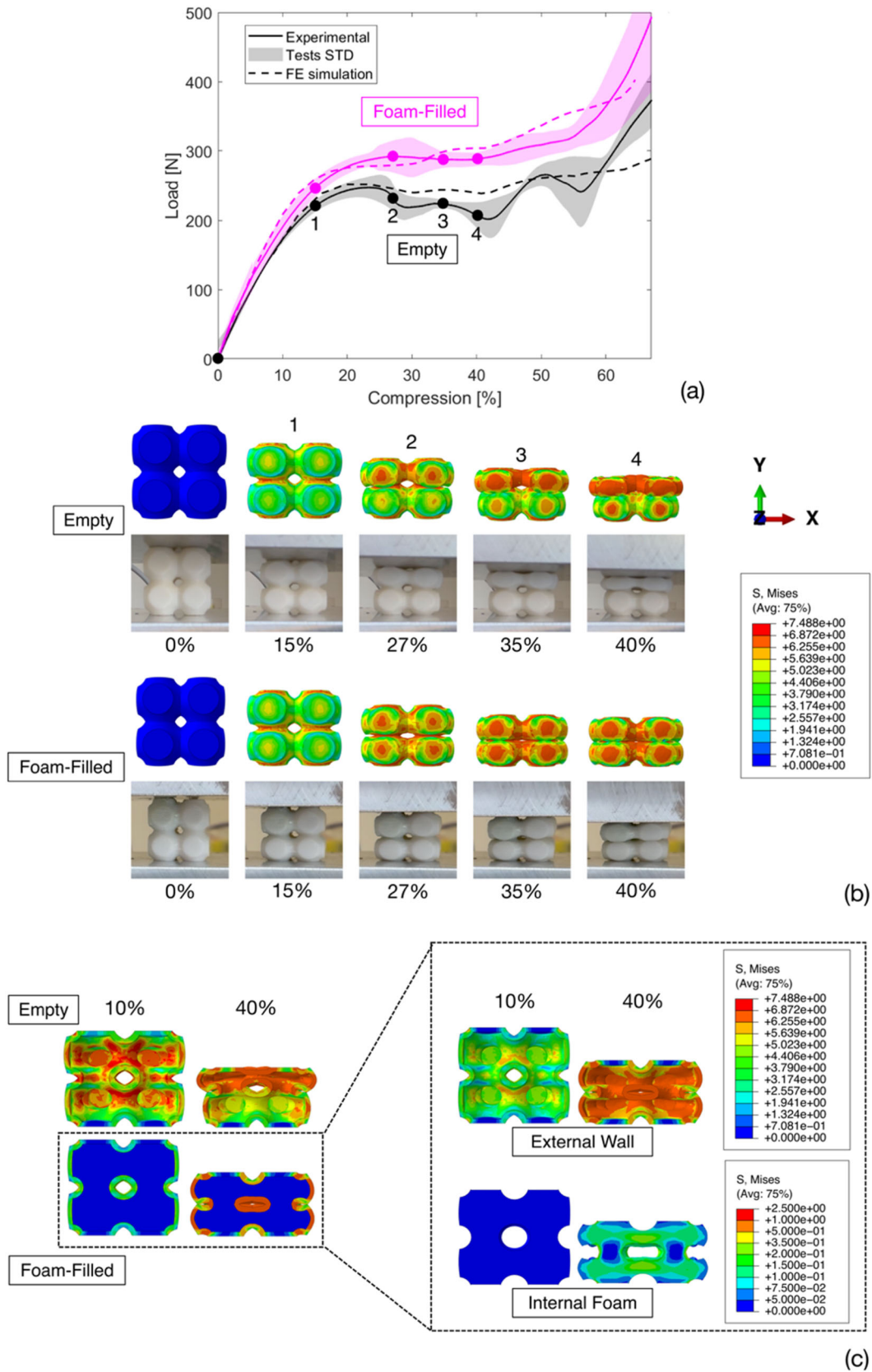
Figure 5. a) Quasi-static compression of empty and FF configurations; b) Stress distribution at different levels of compression; c) Wall and foam contributions.

strength of the foam itself, which is almost two orders of magnitude less than that of the wall, as shown in Figure 5c.

To provide a more in-depth understand of the stress distribution within the structures, as well as the influence of foam on the local stress field in specific regions, a path was defined through the wall thickness at the center of the external wall, as shown in Figure 7a, where the maximum value of stress was attained. Figure 7b shows that, while for small
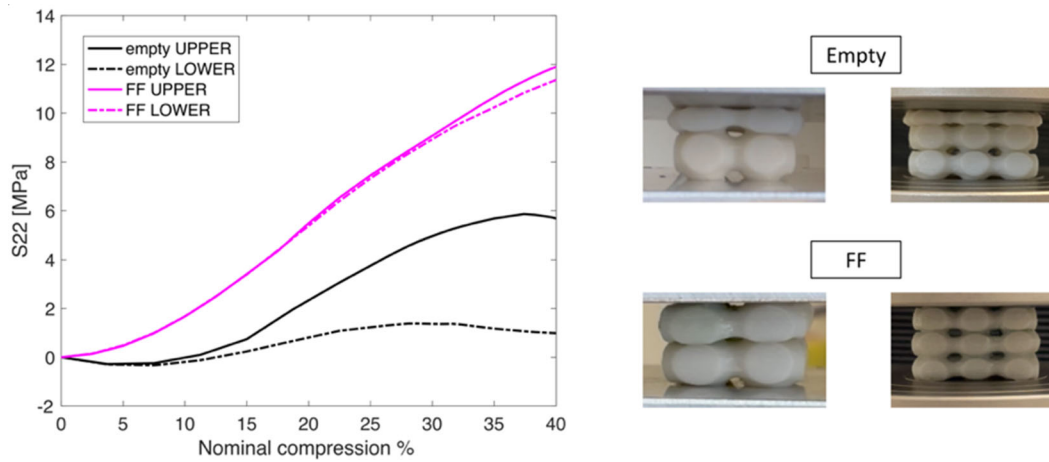
Figure 6. Regularization of the stress field and deformation resulting from foam filling.

levels of nominal compression the stress distributions of the empty and FF configurations were almost the same, for higher values (35% nominal compression) the difference became significant with different macroscopic deformation of the structures, as shown previously in Figure 6.

Figure 7c compares the upper and lower layers at 35% nominal compression, providing data to support the stress regularization effect leading to smoothing of the deformation curve during experiments. Focusing on the continuous red line displaying the axial stress in the upper layer, it can be observed that in the FF configuration the walls undergo only compressive stress (from 0 to $-5\,\text{MPa}$) while for the empty configuration the material enters a bending stress state with a much more significant gradient ($+4\,\text{MPa}$ and $-12\,\text{MPa}$ at the path boundaries).

3.2. Energy absorption performance

Filling the structure with a secondary soft material not only produced an increase in the overall compressive performance but also generated a more isotropic response at a macro-scale, as discussed in Section Static loading and stress field investigation. Further to this beneficial effect, the TEA (and also TED) of the FF configuration was much higher than the sum of the individual contributions of the constituents, PBAT and PU foam. This phenomenon was also observed in [32–33], justifying investigation into foam-filled cellular structures. The green areas in Figure 8a and 8b highlight the significance of interactions between the wall and foam within the FF structure. This unique behavior can again be accounted for in terms of more regular deformation during compression. Filling of cellular structures subject to compressive stresses with foam prevents instability phenomena, leading to a deformation mode that limits the onset of buckling, resulting in a more stable mechanical response. Again, the FF load-displacement curve exhibits a linear "plateau" region, contrary to what is observed in the empty configuration. The reason for this is that the empty structure exhibits irregular behavior due to instability phenomena within layers. Thus, the soft filler acts more as a

regularizer for the behavior of the stronger scaffold than as a load carrier itself.

A comparison of the specific energy absorption is shown in Figure 8c. The FF configuration exhibits an 18% increase in SEA capability compared to the empty configuration. This positive outcome is mainly due to the interaction effect between the two phases, clearly highlighted in Figure 8c.

During cyclic loading testing, both empty and FF configurations underwent compression levels of up to 75% of the nominal height, using the same test parameters as quasi-static monotonic tests. The TED, previously defined in Equation (3), is represented by the area enclosed between the loading and unloading curves in the load-displacement plot. Figure 9a compares the cyclic response of the two configurations after the first loading cycle. A significant increase in the total energy dissipation capability, normalized in terms of mass, can be observed in Figure 9b. Such an improvement is strongly sought after as a beneficial effect of secondary filler materials within thin external shells and can be easily explained by considering the points discussed in Section Static loading and stress field investigation, together with the hysteretic properties of PU foam, which are not unusual amongst hyper-elastic materials.

The SED gained more than 18% with the presence of foam, while the SDC increased by more than 6%. The latter was not very high as the unloading response was similar in both configurations, as can be seen in Figure 9a. The FF configuration increased the load bearing capacity compared with the empty configuration, providing the same increase in TED and TEA, with the effective enhancement of SDC not able to reach very high values.

3.3. Scalability of results

The validation method for sample representativety discussed in Section Sample representativity led to successful outcomes. By observing Figure 10b, it can be seen that the TEA per unit cell was almost independent of the number of cells when considering the 2x2x2 and 3x3x3 cellular structures shown in Figure 10a, implying that the structure was scalably and behavior did not change significantly with size.
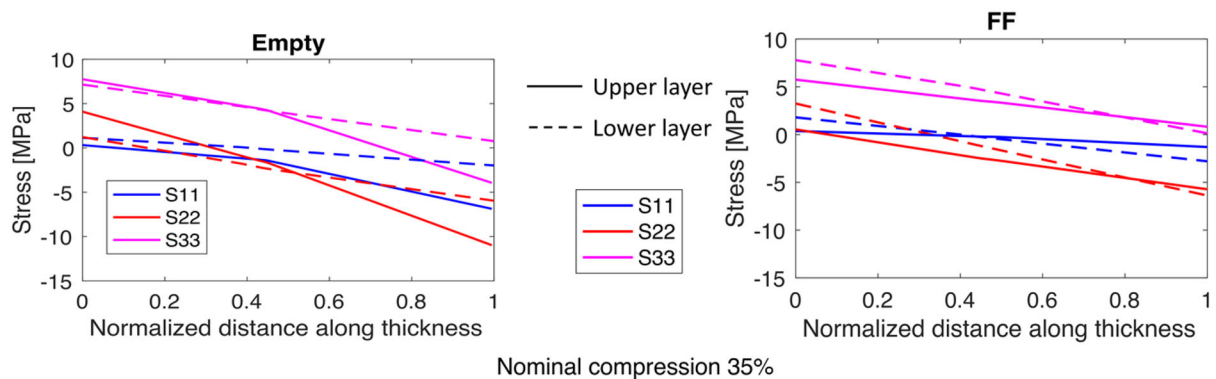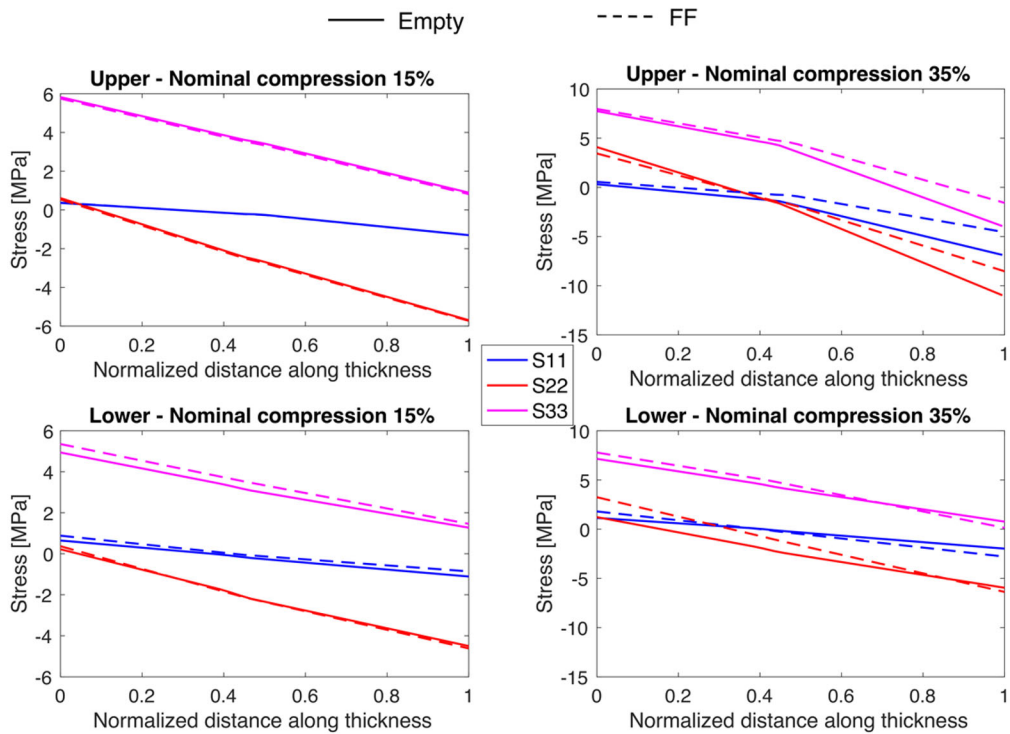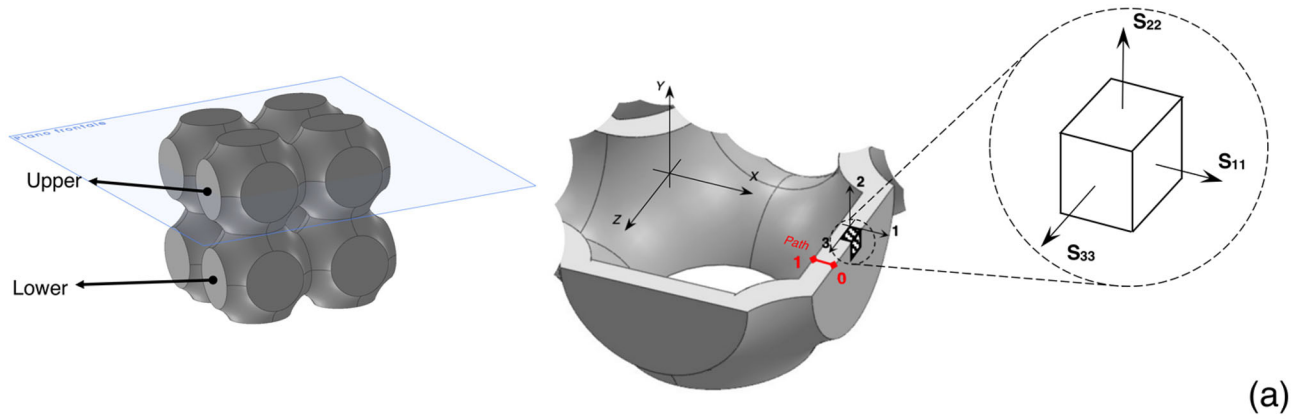
Figure 7. a) Path along wall thickness used for analysis; b) Comparison of the stress distribution along the path at different levels of nominal compression; c) Effect of Foam on stress regularization.

The effect of foam filling was therefore similar for all configurations, enhancing the energy absorption capability on average by 17%.

The initial stiffness was also constant across different sizes, with structures behaving as linear elastic springs and scaling effects having a negligible effect on the compressive response. Moreover, plateau stress results were also found to be independent of the number of cells, with increases in performance also observed for larger structures upon injection of the secondary material, as shown in Figure 10c. The
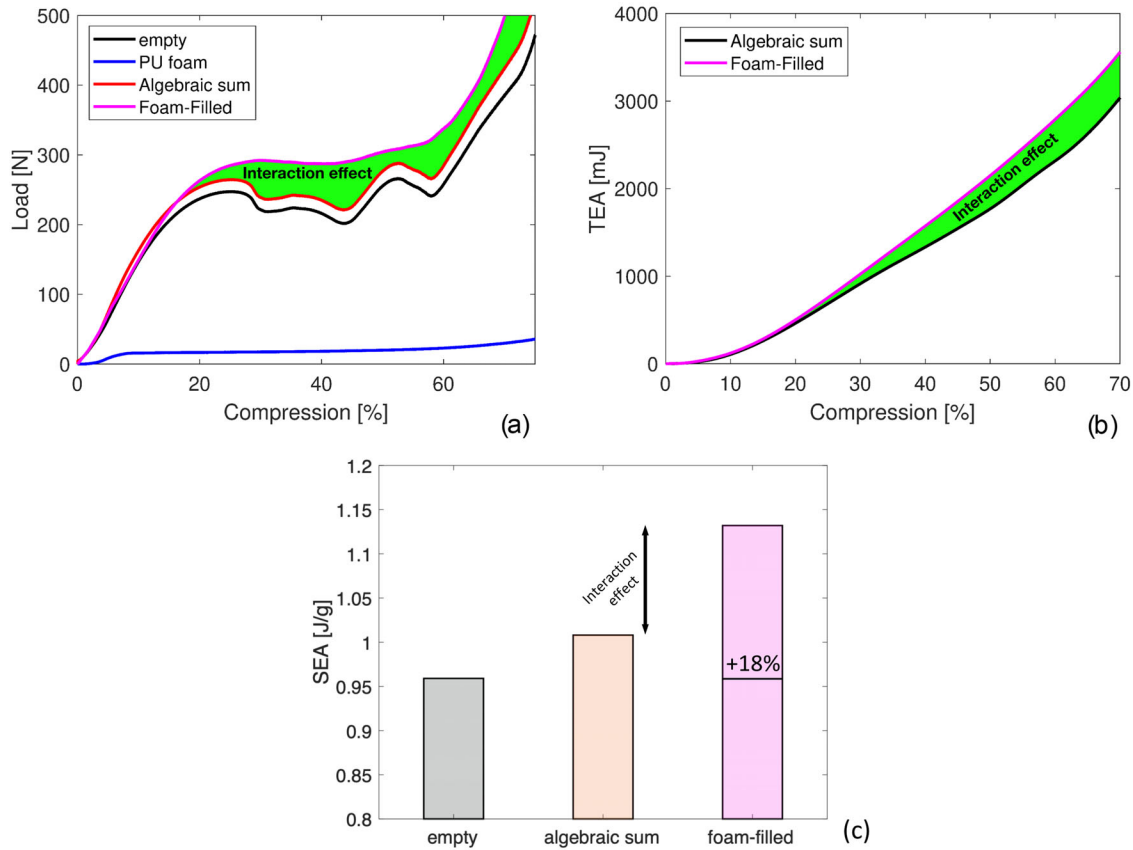
Figure 8. Interaction between the external structure and foam: a) Increased compressive performance; b) Enhanced total energy absorption; c) Comparison of the specific energy absorption.
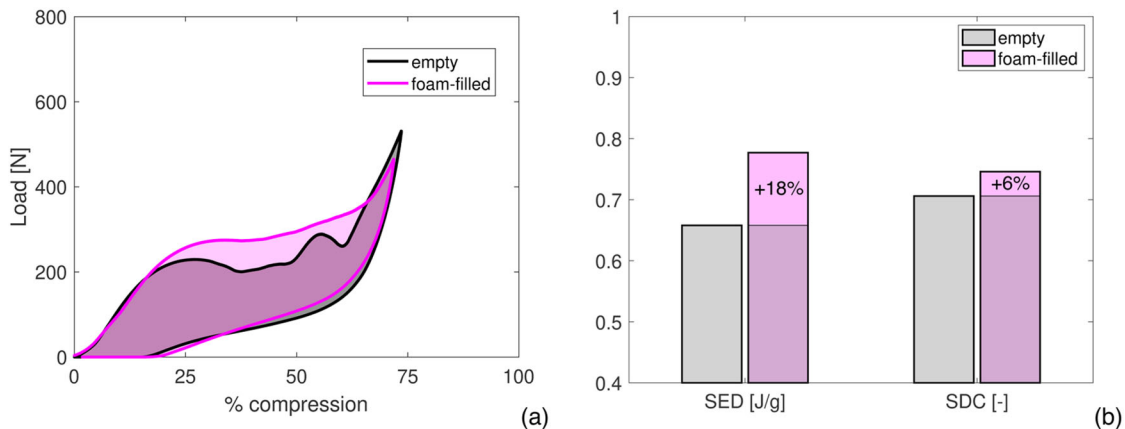
Figure 9. a) Cyclic loading in empty and FF configurations; b) Influence of foam filling on SEA and SDC.

average plateau stress in the FF configuration, defined as the mean of the plateau stress of 8-cell and 27-cell structures, was about 30% higher than that of the original configuration.

This is an encouraging result, as it proves that foam on the one hand delays the occurrence of plasticity in the external shell material, while on the other it reduces anisotropy, leading to a more regular and uniform response.

Finally, experimental results obtained for the FF metamaterial and original cells are reported in Figure 11 in the form of an Ashby map presenting the Specific Energy Absorbtion performance of engineering materials as a function density. Data obtained within the present study falls within the lattice-structure region; specifically, at the top of

the region for nonmetallic materials, confirming the advantages of such structures.

4. Conclusions

The present work has investigated the effect of injecting a secondary soft material on the compressive response of biopolymeric lattice structures. Comparing the mechanical response of the original, empty configuration with that of the same structure filled with PU expandable foam, positive results were observed in terms of both static and cyclic behavior. Numerical simulations were performed to support experiments, with excellent agreement obtained between the two. The outcomes of these
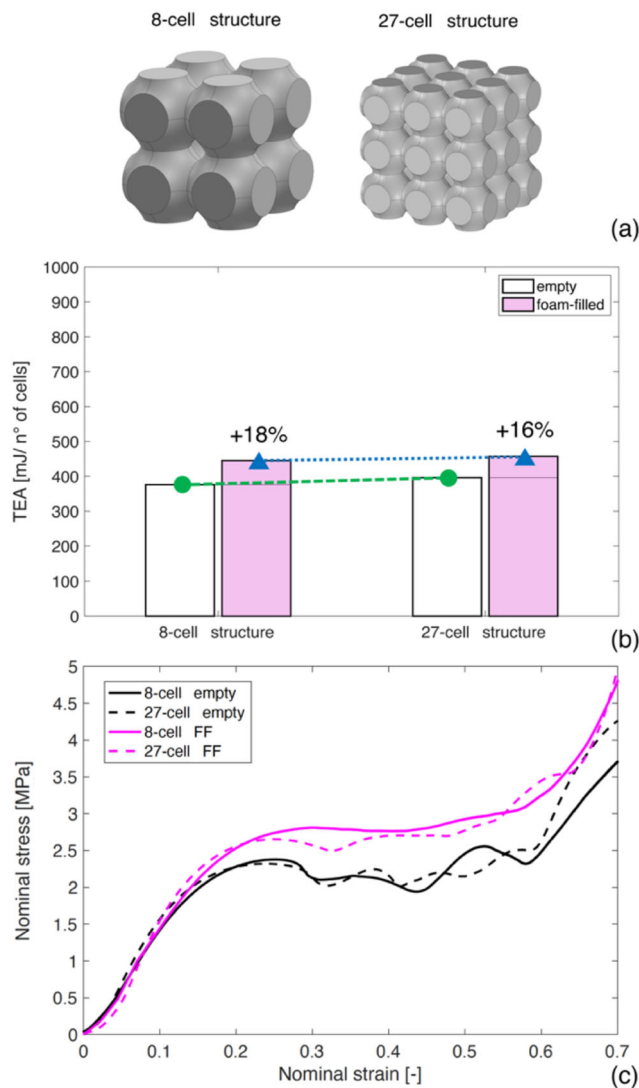
Figure 10. Scalability of the cellular structure: a) Geometry of specimens; b) Energy absorption per unit cell; c) Initial stiffness and plateau stress for different sizes.
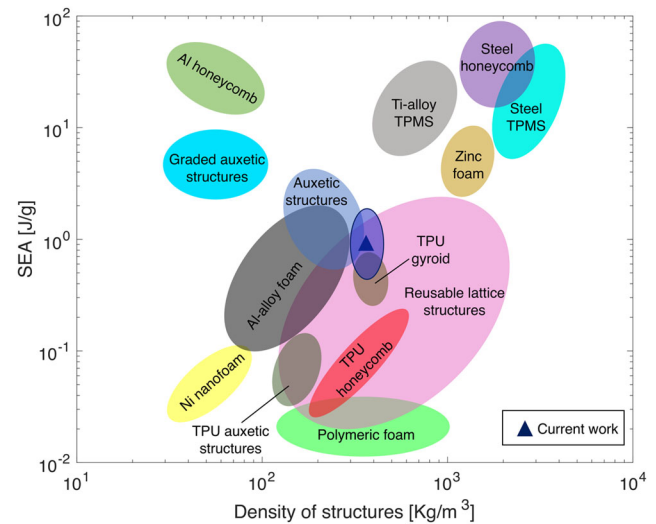

Figure 11. Ashby map with data from current study and the literature [44].

- The effect of foam is very benefitial when considering both the overall load-bearing capacity and energy absorption capability, with plateau stress increasing by 30% and average SEA increasing by 18%;
- The new functionalized meta-material places itself amongst the best lattices in terms of perform.

Finally, the proven biodegradability and good mechanical behavior of PBAT polymer could pave the pathway to new applications for 3D-printed mechanical metamaterials. This could include, for example, energy absorbers and dampers within food packaging to facilitate transition toward plastic-free materials, or biodegradabile scaffolds for tissue rigeneration in biomechanics.

Future works will compare different TPMS and lattice geometries to evaluate how the presence of foam contributes to the amount of local deformation in different bending- or stretch-dominated structures.

simulations demonstrated the reproducibility of the compressive response of such structures and provided insight into the resulting stress distribution and its influence on the deformation of the entire structure in each case. Scalability of the structure was also demonstrated, allowing generalization of results and theory to a wider range of applications.

The main findings of the work are as follows:

- PBAT achieves good mechanical properties and good printability, paving the way to more environmentally sustainable production thanks to its demonstrated biodegradability;
- Filling thin-walled structures with a secondary foam-like material leads to an increase in compressive preformance thanks to interaction between the two constituents, combining the good properties of lattices produced by additive manufacturing and the functional effect of PU foam;
- Foam-filled periodic structures exhibit more uniform and regular deformation when subjected to compression, contrasting the buckling of some cells, which is responsible for a drop in strength of empty structures;

Disclsoure statement

No potential conflict of interest was reported by the author(s).

ORCID

A. Corvi (iD) http://orcid.org/0000-0002-2129-8155
L. Collini (iD) http://orcid.org/0000-0002-1497-9470
C. Sciancalepore (iD) http://orcid.org/0000-0002-8182-6618

References

[1] J. Fan, L. Zhang, S. Wei, Z. Zhang, S.-K. Choi, B. Song, and Y. Shi, A review of additive manufacturing of metamaterials and developing trends, Mater. Today., vol. 50, pp. 303–328, 2021. DOI: 10.1016/j.mattod.2021.04.019.

[2] D. Sharma, and S.S. Hiremath, Additively manufactured mechanical meta materials based on triply periodic minimal surfaces: performance, challenges, and application, Mech. Adv. Mater. Struct., vol. 29, no. 26, pp. 5077–5107, 2022. DOI: 10.1080/15376494.2021.1948151.

[3] R. Miralbes, D. Ranz, F. J. Pascual, D. Zouzias, and M. Maza, Characterization of additively manufactured triply periodic minimal surface structures under compressive loading, Mech. Adv. Mater. Struct., vol. 29, no. 13, pp. 1841–1855, 2022. DOI: 10.1080/15376494.2020.1842948.

[4] R. Noroozi, F. Tatar, A. Zolfagharian, R. Brighenti, M.A. Shamekhi, A. Rastgoo, A. Hadi, and M. Bodaghi, Additively manufactured multi-morphology bone-like porous scaffolds: experiments and micro-computed tomography-based finite element modeling approaches, Int J Bioprint., vol. 8, no. 3, pp. 556, 2022. DOI: 10.18063/ijb.v8i3.556.

[5] B. Yilmaz, Additive manufacturing and characterization of mathematically designed bone scaffolds based on triply periodic minimal surface lattices, Mech. Adv. Mater. Struct., pp. 1–11, 2023. DOI: 10.1080/15376494.2023.2177913.

[6] J. Li, H. Guo, P. Sun, Y. Wang, S. Huang, T. Yuan, and H. Zhang, Topology optimisation of anisotropy hierarchal honeycomb acoustic meta materials for extreme multi-broad band gaps, Mech. Adv. Mater. Struct., vol. 30, no. 17, pp. 3540–3552, 2023. DOI: 10.1080/15376494.2022.2079027.

[7] J.U. Surjadi, L. Gao, H. Du, X. Li, X. Xiong, N.X. Fang, and Y. Lu, Mechanical metamaterials and their engineering applications, Adv. Eng. Mater., vol. 21, no. 3, pp. 1800864, 2019. DOI: 10.1002/adem.201800864.

[8] S. Shan, S.H. Kang, J.R. Raney, P. Wang, L. Fang, F. Candido, J.A. Lewis, and K. Bertoldi, Multistable architected materials for trapping elastic strain energy, Adv. Mater., vol. 27, no. 29, pp. 4296–4301, 2015. DOI: 10.1002/adma.201501708.

[9] F. Ghorbani, H. Gharehbaghi, A. Farrokhabadi, A. Bolouri, A.H. Behravesh, and S.K. Hedayati, Investigation of energy absorption performances of a 3D printed fibre-reinforced bio-inspired cellular structure under in-plane compression loading, Mech. Adv. Mater. Struct., pp. 1–19, 2023. DOI: 10.1080/15376494.2023.2214552.

[10] Y. Chen, L. Ye, C. Xu, and Y.X. Zhang, Multi-material topology optimisation of micro-composites with reduced stress concentration for optimal functional performance, Materials & Design., vol. 210, pp. 110098, 2021. DOI: 10.1016/j.matdes.2021.110098.

[11] D.H. Werner, J.A. Bossard, Z. Bayraktar, Z.H. Jiang, M.D. Gregory, and P.L. Werner, Nature inspired optimization techniques for metamaterial design. In: Numerical Methods for Metamaterial Design. Topics in Applied Physics, vol. 127., K. Diest, ed., Dordrecht: Springer. 2013.

[12] A. Corvi, L. Collini, C. Sciancalepore, and A. Kumar, Analysis and modelling of damage mechanism in FDM 3D-printed lattice structure under compression loading, J Mech Sci Technol., vol. 37, no. 3, pp. 1089–1095, 2023. DOI: 10.1007/s12206-022-2104-4.

[13] A. Kumar, L. Collini, A. Daurel, and J.-Y. Jeng, Design and additive manufacturing of closed cells from supportless lattice structure, Addit. Manuf., vol. 33, pp. 101168, 2020. DOI: 10.1016/j.addma.2020.101168.

[14] L. Collini, C. Ursini, and A. Kumar, Design and optimization of 3D fast printed cellular structures, Mat Design & Process Comms., vol. 3, no. 4, pp. e227, 2021. DOI: 10.1002/mdp2.227.

[15] Z. Huang, B. Li, L. Ma, and Y. Li, Mechanical properties and energy absorption performance of bio-inspired dual architecture phase lattice structures, Mech. Adv. Mater. Struct., vol. 30, no. 9, pp. 1842–1852, 2023. DOI: 10.1080/15376494.2022.2045654.

[16] G. Dong, D. Tessier, and Y.F. Zhao, Design of shoe soles using Lattice Structures fabricated by Additive Manufacturing, in Proceedings of the 22nd International Conference on Engineering Design (ICED19), Delft, The Netherlands, 5–8. August 2019.

[17] J.J. Andrew, P. Verma, and S. Kumar, Impact behavior of nano-engineered, 3D printed plate-lattices, Mater. Des., vol. 202, pp. 109516, 2021. DOI: 10.1016/j.matdes.2021.109516.

[18] Y.-T. Kao, A.R. Amin, N. Payne, J. Wang, and B.L. Tai, Low-velocity impact response of 3D-printed lattice structure with foam reinforcement, Compos. Struct., vol. 192, pp. 93–100, 2018. DOI: 10.1016/j.compstruct.2018.02.042.

[19] M. Khodaei, M.S. Farahani, and M. Haghighi-Yazdi, Numerical investigation of high velocity impact on foam-filled honeycomb structures including foam fracture model, Mech. Adv. Mater. Struct., vol. 29, no. 5, pp. 748–760, 2022. DOI: 10.1080/15376494.2020.1793239.

[20] H. Yin, G. Wen, Z. Liu, and Q. Qing, Crashworthiness optimization design for foam-filled multi-cell thin-walled structures, Thin. Walled Struct., vol. 75, pp. 8–17, 2014. DOI: 10.1016/j.tws.2013.10.022.

[21] Ali Ghamarian, Hamid Reza Zarei, and Mohammad Taha Abadi, Experimental and numerical crashworthiness investigation of empty and foam-filled end-capped conical tubes, Thin. Walled Struct., vol. 49, no. 10, pp. 1312–1319, 2011. DOI: 10.1016/j.tws.2011.03.005.

[22] Hozhabr Mozafari, Soroush Khatami, Habibollah Molatefi, Vincenzo Crupi, Gabriella Epasto, and Eugenio Guglielmino, Finite element analysis of foam-filled honeycomb structures under impact loading and crashworthiness design, Int. J. Crashworthiness., vol. 21, no. 2, pp. 148–160, 2016. DOI: 10.1080/13588265.2016.1140710.

[23] Ru-Yang Yao, Bei Zhang, Guan-Sheng Yin, and Zhen-Yu Zhao, Energy absorption behaviors of foam-filled holed tube subjected to axial crushing: experimental and theoretical investigations, Mech. Adv. Mater. Struct., vol. 28, no. 24, pp. 2501–2514, 2021. DOI: 10.1080/15376494.2020.1745968.

[24] Amin Farrokhabadi, Hossein Veisi, Hussain Gharehbaghi, John Montesano, Amir Hossein Behravesh, and Seyyed Kaveh Hedayati, Investigation of the energy absorption capacity of foam-filled 3D-printed glass fiber reinforced thermoplastic auxetic honeycomb structures, Mech. Adv. Mater. Struct., vol. 30, no. 4, pp. 758–769, 2023. DOI: 10.1080/15376494.2021.2023919.

[25] F.H. Roudbeneh, Experimental investigation of quasistatic penetration tests on honeycomb sandwich panels filled with polymer foam, Mech. Adv. Mater. Struct., vol. 27, no. 21, pp. 1803–1815, 2020.

[26] Samuel Black, Antzela Tzagiollari, Subrata Mondal, Nicholas Dunne, and David B. MacManus, Mechanical behaviour of gel-filled additively-manufactured lattice structures under quasi-static compressive loading, Mater. Today Commun., vol. 35, pp. 106164, 2023. DOI: 10.1016/j.mtcomm.2023.106164.

[27] Gaojian Lin, Jiaqi Li, Fei Li, Pengwan Chen, and Weifu Sun, Low velocity impact response of sandwich composite panels with shear thickening gel filled honeycomb cores, Compos. Commun., vol. 32, pp. 101136, 2022. DOI: 10.1016/j.coco.2022.101136.

[28] S. She, Investigating the dynamic compression response of elastomeric, additively manufactured fluid-filled structures via experimental and finite element analyses, Addit. Manuf., vol. 39, pp. 101885, 2021.

[29] Z. Wang, R. Bo, H. Bai, S. Cao, S. Wang, J. Chang, Y. Lan, Y. Li, and Y. Zhang, Flexible impact-resistant composites with bio-inspired three-dimensional solid-liquid lattice designs, ACS Appl Mater Interfaces., vol. 15, no. 18, pp. 22553–22562, 2023. DOI: 10.1021/acsami.3c02761.

[30] N.V. Gama, A. Ferreira, and A. Barros-Timmons, Polyurethane foams: past, Present, and Future, Materials., vol. 11, no. 10, pp. 1841, 2018. DOI: 10.3390/ma11101841.

[31] T. Liu, C. Chen, and Y. Cheng, Mechanical characteristics and foam filling enhancement mechanism of polymeric periodic hybrid structures under uniaxial compression, Materials & Design., vol. 227, pp. 111762, 2023. DOI: 10.1016/j.matdes.2023.111762.

[32] R. Yao, T. Pang, S. He, Q. Li, B. Zhang, and G. Sun, A bio-inspired foam-filled multi-cell structural configuration for energy absorption, Composites Part B., vol. 238, pp. 109801, 2022. DOI: 10.1016/j.compositesb.2022.109801.

[33] X. Ren, Y. Zhang, C.Z. Han, D. Han, X.Y. Zhang, X.G. Zhang, and Y.M. Xie, Mechanical properties of foam-filled auxetic circular tubes: experimental and numerical study, Thin. Walled Struct., vol. 170, pp. 108584, 2022. DOI: 10.1016/j.tws.2021.108584.

[34] A. Airoldi, N. Novak, F. Sgobba, A. Gilardelli, and M. Borovinšek, Foam-filled energy absorbers with auxetic behavior for localized impacts, Materials Science & Engineering A., vol. 788, pp. 139500, 2020. DOI: 10.1016/j.msea.2020.139500.

[35] H.C. Luo, X. Ren, Y. Zhang, X.Y. Zhang, X.G. Zhang, C. Luo, X. Cheng, and Y.M. Xie, Mechanical properties of foam-filled hexagonal and re-entrant honeycombs under uniaxial compression, Compos. Struct., vol. 280, pp. 114922, 2022. DOI: 10.1016/j.compstruct.2021.114922.

[36] N. Novak, O. Al-Ketan, L. Krstulović-Opara, R. Rowshan, M. Vesenjak, and Z. Ren, Bending behavior of triply periodic minimal surface foam-filled tubes, Mech. Adv. Mater. Struct., vol. 30, no. 15, pp. 3061–3074, 2023. DOI: 10.1080/15376494.2022.2068207.

[37] R. Miralbes, F.J. Pascual, D. Ranz, and J.A. Gomez, Mechanical properties of hybrid structures generated by additively manufactured triply periodic minimal surface structures and foam, Mech. Adv. Mater. Struct., pp. 1–12, 2022. DOI: 10.1080/15376494.2022.2092797.

[38] M.J. Prajapati, A. Kumar, S.-C. Lin, and J.-Y. Jeng, Multi-material additive manufacturing with lightweight closed-cell foam-filled lattice structures for enhanced mechanical and functional properties, Addit. Manuf., vol. 54, pp. 102766, 2022. DOI: 10.1016/j.addma.2022.102766.

[39] C. Sciancalepore, E. Togliatti, A. Giubilini, D. Pugliese, F. Moroni, M. Messori, and D. Milanese, Preparation and characterization of innovative poly(butylene adipate terephthalate)-based biocomposites for agri-food packaging application, J of Applied Polymer Sci., vol. 139, no. 24, pp. 52370, 2022. DOI: 10.1002/app.52370.

[40] C. Sciancalepore, E. Togliatti, M. Marozzi, F.M.A. Rizzi, D. Pugliese, A. Cavazza, O. Pitirollo, M. Grimaldi, and D. Milanese, Flexible PBAT-Based composite filaments for tunable FDM 3D Printing, ACS Appl Bio Mater., vol. 5, no. 7, pp. 3219–3229, 2022. DOI: 10.1021/acsabm.2c00203.

[41] L.J. Gibson, and M.F. Ashby, Cellular Solids, Cambridge University Press, Cambridge, 1997.

[42] E. Togliatti, D. Milanese, D. Pugliese, and C. Sciancalepore, Viscoelastic characterization and degradation stability investigation of Poly(butylene-adipate-co-terephthalate) – Calcium-Phosphate Glass composites, J Polym Environ., vol. 30, no. 9, pp. 3914–3933, 2022. DOI: 10.1007/s10924-022-02479-1.

[43] A. Pietrosanto, P. Scarfato, L.D. Maio, and L. Incarnato, Development of Eco-Sustainable PBAT-Based blown films and performance analysis for food packaging applications, Materials., vol. 13, no. 23, pp. 5395, 2020. DOI: 10.3390/ma13235395.

[44] D. Sharma, and S.S. Hiremath, Bio-inspired repeatable lattice structures for energy absorption: experimental and finite element study, Composites Structures., vol. 283, pp. 115102, 2022. DOI: 10.1016/j.compstruct.2021.115102.